JOURNAL OF GEOPHYSICAL RESEARCH, VOL. 113, D18309, doi:10.1029/2008JD009854, 2008

Contribution of stratospheric ozone to the interannual variability of tropospheric ozone in the northern extratropics

Yukio Terao,[1,2] Jennifer A. Logan,[1] Anne R. Douglass,[3] and Richard S. Stolarski[3]

Received 23 January 2008; revised 17 April 2008; accepted 18 June 2008; published 24 September 2008.

[1] We examined the role of variability in the input of stratospheric ozone on the interannual variability of tropospheric ozone in the northern extratropics using correlations of monthly ozone anomalies for the lower stratosphere and the troposphere. We used output from a multiyear simulation of the NASA Goddard Space Flight Center (GSFC) Chemistry and Transport Model (CTM), and evaluated model results using ozonesonde data. The GSFC CTM explicitly calculates stratospheric ozone and simulates separate tracers of stratospheric and tropospheric ozone (O_3-strat and O_3-trop, respectively). The climatological seasonal cycle of ozone shows that O_3-strat contributes significantly to the spring maximum of ozone at 500 hPa, ~40% at high latitudes and ~30% at midlatitudes. We find large regional differences in the correlation of ozone in the lower stratosphere and troposphere in the model that are supported by the ozonesonde data. Highest correlations are found from the eastern Atlantic to Europe, from the eastern Pacific to the western United States, and over the polar regions, in winter-spring. This spatial pattern is due to the input of O_3-strat into the troposphere. The distribution and time lag of the correlations (highest with no lag for midlatitudes and a 1–2 month lag for polar regions) are consistent with the dynamical indicators of stratosphere-troposphere exchange (STE), such as storm tracks in the midlatitudes and slow descending motion in the polar region. Our simple approach can be widely applied to diagnose the effect of STE on tropospheric ozone.

Citation: Terao, Y., J. A. Logan, A. R. Douglass, and R. S. Stolarski (2008), Contribution of stratospheric ozone to the interannual variability of tropospheric ozone in the northern extratropics, *J. Geophys. Res.*, *113*, D18309, doi:10.1029/2008JD009854.

1. Introduction

[2] Recent analyses imply that interannual variability and trends in tropospheric ozone are influenced by those in lower stratospheric ozone. Following anomalously low ozone in the lower stratosphere after the eruption of Mt. Pinatubo in June, 1991, tropospheric ozone was also low in 1992–1993, as shown by ozonesonde measurements at northern midlatitude stations [*Fusco and Logan*, 2003]. *Tarasick et al.* [2005] examined Canadian ozonesonde data and showed that annual-mean tropospheric ozone levels were correlated with ozone in the lower stratosphere. *Ordóñez et al.* [2007] found high correlations between lower stratospheric ozone and surface ozone at mountain-top sites in Europe using 12 month running means; correlations were strongest in spring. These studies investigated limited regions and used highly smoothed data. Here we examine correlations in interannual variability of tropospheric ozone and lower stratospheric ozone with more extensive observations and with results from a global model.

[3] The two sources of tropospheric ozone are transport from the stratosphere and photochemical production in the troposphere. Recent models imply that the stratospheric source of ozone is 550 ± 170 Tg and that the photochemical tropospheric source is 5100 ± 600 Tg for a year 2000 simulation [*Stevenson et al.*, 2006]. The flux of ozone from the stratosphere to the troposphere is highest in March-July [*Olsen et al.*, 2004] but model simulations with "tagged" sources show that the stratospheric source has the largest effect on tropospheric ozone mixing ratios in winter-spring when the ozone lifetime is longer [e.g., *Lelieveld and Dentener*, 2000; *Fusco and Logan*, 2003; *Sudo and Akimoto*, 2007]. All these previous studies used tropospheric chemistry and transport models (CTMs); stratospheric input was derived by relaxing ozone concentrations to observations, or by using an artificial tracer. Here we use a model that simulates stratospheric chemistry and transport [*Stolarski et al.*, 2006].

[4] Trends in tropospheric ozone in recent decades reveal spatially and temporally inhomogeneous patterns [*Logan et al.*, 1999; *Oltmans et al.*, 2006; *World Meteorological Organization* (*WMO*), 2007]. In the middle troposphere, ozone increased over Europe from the late 1960s until the middle 1980s, but has not increased since then, although

[1] School of Engineering and Applied Sciences, Harvard University, Cambridge, Massachusetts, USA.
[2] Now at Center for Global Environmental Research, National Institute for Environmental Studies, Tsukuba, Japan.
[3] Atmospheric Chemistry and Dynamics Branch, NASA Goddard Space Flight Center, Greenbelt, Maryland, USA.

0148-0227/08/2008JD009854$09.00

there are periods with decreases and increases [*Logan et al.*, 1999; *Oltmans et al.*, 2006; *Zbinden et al.*, 2006]. Mountaintop measurements show an increase in ozone for 1992–2004 in central Europe [*Ordóñez et al.*, 2007]. Data for Japan show an increase in the 1970s, but little change since then [*Logan et al.*, 1999; *Oltmans et al.*, 2006]. By contrast, there has been no trend in ozone over the United States, and a decrease over Canada up to 1993 [*Logan et al.*, 1999]. *Tarasick et al.* [2005] show that tropospheric ozone has been increasing at all Canadian sonde stations since 1991. *Fusco and Logan* [2003] show that it is difficult to reconcile past changes with current understanding. One area of particular uncertainty is the role of stratospheric input in influencing the distribution and trends of tropospheric ozone, masking the effects of increased emissions of ozone precursors.

[5] The purpose of this study is to examine the role of variability in the input of stratospheric ozone on the interannual variability of tropospheric ozone. We use output from a multiyear simulation of the GSFC CTM. This simulation is well suited for our purpose. *Stolarski et al.* [2006] show that the model produces realistic variability and trends in stratospheric ozone. *Olsen et al.* [2004] show that the model produces realistic cross-tropopause fluxes of mass and ozone. Finally, the simulation includes separate tracers for ozone of tropospheric and stratospheric origin. We first evaluate the seasonal cycle of tropospheric ozone in the model and show the amount that is transported from the stratosphere. Our major focus is then to present a new but simple way to assess the contribution of variability in stratospheric ozone to that in tropospheric ozone by correlating monthly anomaly ozone time series for the lower stratosphere and the troposphere; we evaluate our results using ozonesonde data.

2. Data

2.1. Ozonesonde

[6] We used ozonesonde data from 12 long-term stations in the northern extratropics. Ozonesonde data were obtained from the World Ozone and Ultraviolet Radiation Data Centre (WOUDC) for Uccle (station code 053, 51°N, 4°E), Hohenpeissenberg (099, 48°N, 11°E), and Payerne (156, 47°N, 7°E) in Europe; Tateno (014, 36°N, 140°E), Sapporo (012, 43°N, 141°E), and Kagoshima (007, 32°N, 131°E) in Japan; Resolute (024, 75°N, 95°W), Edmonton (021, 53°N, 114°W), Churchill (077, 59°N, 94°W), and Goose Bay (076, 53°N, 60°W) in Canada; and Wallops Island (107, 38°N, 76°W) in the United States. Recent data for Wallops Island were provided by F. Schmidlin (personal communication, 2005), and data for Boulder (067, 40°N, 105°W) by S. Oltmans (personal communication, 2005). Different types of ozonesondes were used on each continent; electrochemical concentration cell (ECC) sondes for North America, primarily Brewer Mast (BM) sondes for Europe (ECC sondes after 1997 for Uccle and after 2002 for Payerne), and KC sondes for Japan. Further information on data quality issues and on selection criteria for the sonde data is given by *Logan* [1994], *Logan et al.* [1999], and *Terao and Logan* [2007].

[7] The sonde data were processed to give monthly mean values of the column of ozone in Dobson Units (DU) in 33 equally spaced layers in log-pressure from 1000 to 6.3 hPa (~1 km thickness) [*Logan et al.*, 1999]. 1 DU is defined as the column height of pure gaseous ozone in 1×10^{-3} cm at standard pressure and temperature, and is equivalent to 2.687×10^{16} molecules cm^{-2}. In this study we use ozonesonde data for three layers that are ~1 km thick: 200 hPa (from 185 to 215 hPa), 500 hPa (464–541 hPa), and 800 hPa (736–858 hPa). These layers are regarded as the lower stratosphere, midtroposphere, and lower troposphere, respectively.

2.2. Model

[8] We use results of a simulation using the GSFC CTM for 1973–2023 [*Stolarski et al.*, 2006]. The CTM, an updated version of that used by *Douglass et al.* [2003], was driven by meteorological data from a 50-year integration of the Finite-Volume General Circulation Model (FVGCM). The FVGCM is an early version of the Goddard Earth Observing System (GEOS)-4 GCM. The FVGCM was run with resolution of $2° \times 2.5°$ and 55 vertical levels from surface to 0.01 hPa. It uses a flux-form semi-Lagrangian transport code with a quasi-Lagrangian vertical coordinate [*Lin*, 2004], which yields accurate computation of tracer transport [*Lin and Rood*, 1996] and dynamical evolution [*Lin and Rood*, 1997]. Physical tendencies are calculated using a version of the parameterization package of *Kiehl et al.* [1998]. The lower-boundary sea-surface temperatures and sea-ice distributions were imposed from *Rayner et al.* [2003].

[9] The CTM simulation was run with resolution of $2° \times 2.5°$ but with 28 levels from 918 hPa to 0.656 hPa. It also used the numerical transport scheme of *Lin and Rood* [1996]. Boundary conditions for source gases (chlorofluorocarbon, halons, methane, and nitrous oxide) were specified by scenario A2 of *WMO* [2003]. Solar radiation and aerosol distributions up to 2003 were based on observations. The specific details are described by *Stolarski et al.* [2006].

[10] The GSFC CTM and FVGCM have been used for investigations of stratospheric chemistry, ozone trends, and stratosphere-troposphere exchange (STE). *Strahan and Douglass* [2004] showed that a CTM using FVGCM meteorological fields produces a distribution for mean age of stratospheric air that is similar to that derived from observations. *Stolarski et al.* [2006] examined trends of stratospheric ozone in the GSFC CTM run with the FVGCM and showed that the model-derived vertical profile trends for 1980–1996 are similar to observed trends in northern midlatitudes. *Olsen et al.* [2004] examined the exchange of mass and ozone between the stratosphere and troposphere using a subset of the output from the same simulation used here. They showed that the cross-tropopause ozone flux from the stratosphere to the troposphere in the model is ~500 Tg/yr, with a mean of 252 Tg/yr (and a range of 239–273 Tg/yr) in the northern extratropics for model years 1979–1983. The mean flux agrees well with empirically-based estimates, as well as model-based estimates.

[11] In the CTM simulation, ozone that is produced in the stratosphere (referred to as O_3-strat) and ozone that is produced in the troposphere (O_3-trop) are treated as separate tracers. In this paper the term "ozone" for the model output will be used for the sum of O_3-trop and O_3-strat. The GSFC

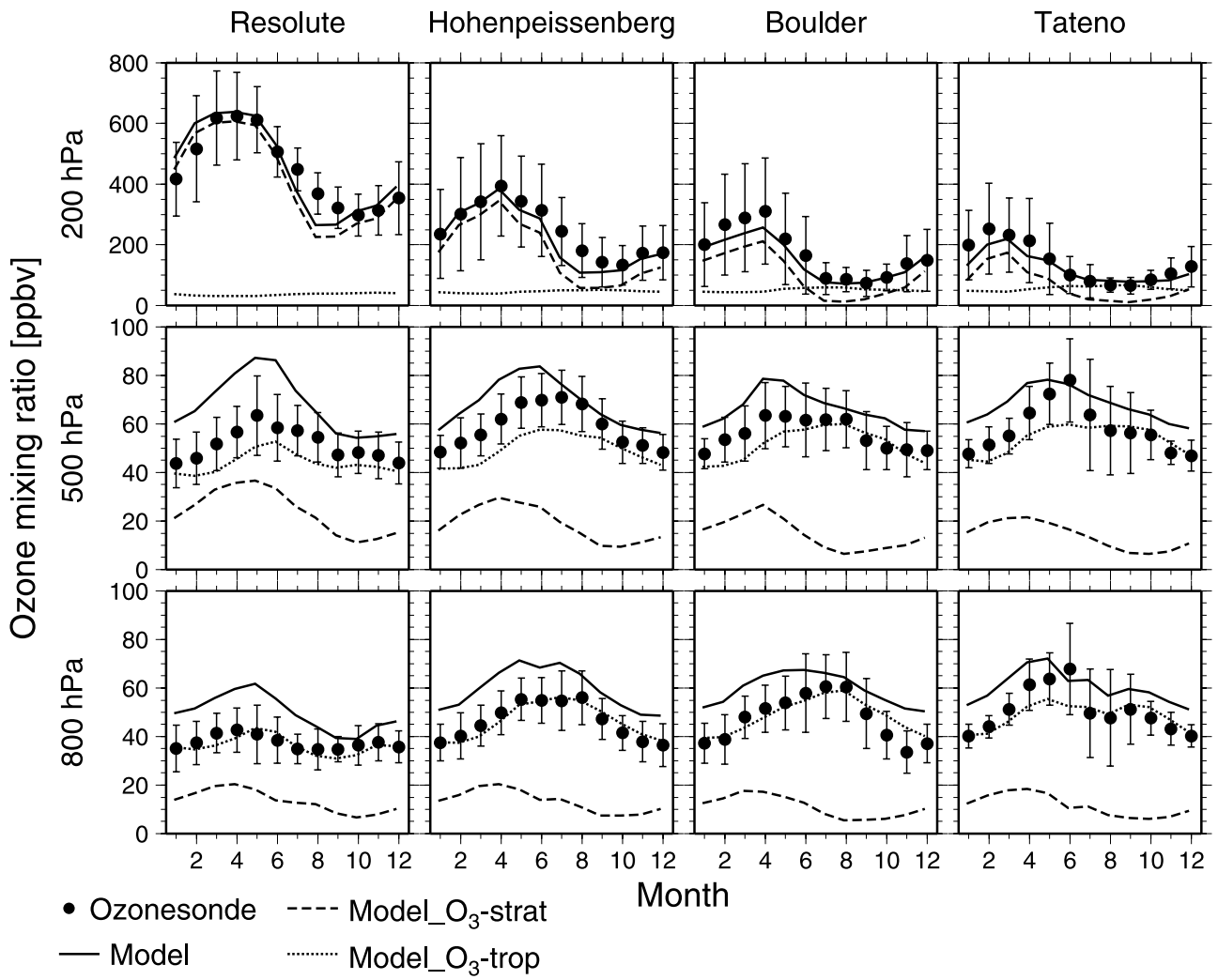

Figure 1. Seasonal cycle of monthly mean ozone from 1985 to 2000 observed by ozonesondes (circles, $\pm 1\sigma$) and calculated by the CTM (solid line) at Resolute, Hohenpeissenberg, Boulder, and Tateno at 200 hPa, 500 hPa, and 800 hPa. Simulated O_3-strat and O_3-trop are shown by dashed and dotted lines, respectively.

CTM explicitly calculates O_3-strat with full stratospheric chemistry including photochemical production/loss processes and parameterization of polar stratospheric clouds and denitrification. Monthly production rates and loss frequencies for the O_3-trop are taken from a simulation for 2001 using the GEOS-Chem model driven by assimilated meteorological fields from the GEOS-3 system [*Fiore et al.*, 2003]. These were used to solve the continuity equation for O_3-trop, and dry deposition was included. The photochemical production and loss terms are the same each model year. The tropospheric simulation was run with one year of convective mass fluxes that are repeated each year. The CTM switches from using the full chemistry scheme for the stratosphere to using the monthly rates for the troposphere at the 2 potential vorticity unit (PVU) surface (1 PVU = 10^{-6} m^2 K kg^{-1} s^{-1}). The O_3-strat that is transported to the troposphere is removed with the same loss rates as O_3-trop; any O_3-trop that is transported to the stratosphere undergoes stratospheric loss.

[12] Output from the 50 year CTM simulation was archived on a $4^\circ \times 5^\circ$ grid for 6 days per month (at 12 UT for days 1, 5, 10, 15, 20, 25 of each month). We use monthly mean mixing ratios (the mean of 6 days) of the O_3-trop and O_3-strat at 188, 543, and 772 hPa (the actual model layers) for the years from 1985 to 2000. The correlation analysis described below used output at these three model layers and ozonesonde data at 200, 500, and 800 hPa, without any vertical interpolation. The results were almost the same even if we used neighboring model layers, so vertical interpolation was unnecessary. An exception is for the climatological analysis of the seasonal cycle of ozone in section 3.1, where we interpolated to the same levels for model evaluation.

[13] We use observed and simulated time series of monthly anomaly (i.e., deseasonalized) ozone for the correlation analysis. Monthly anomalies are the difference between a given monthly mean and the average of all monthly means for that calendar month over the data record

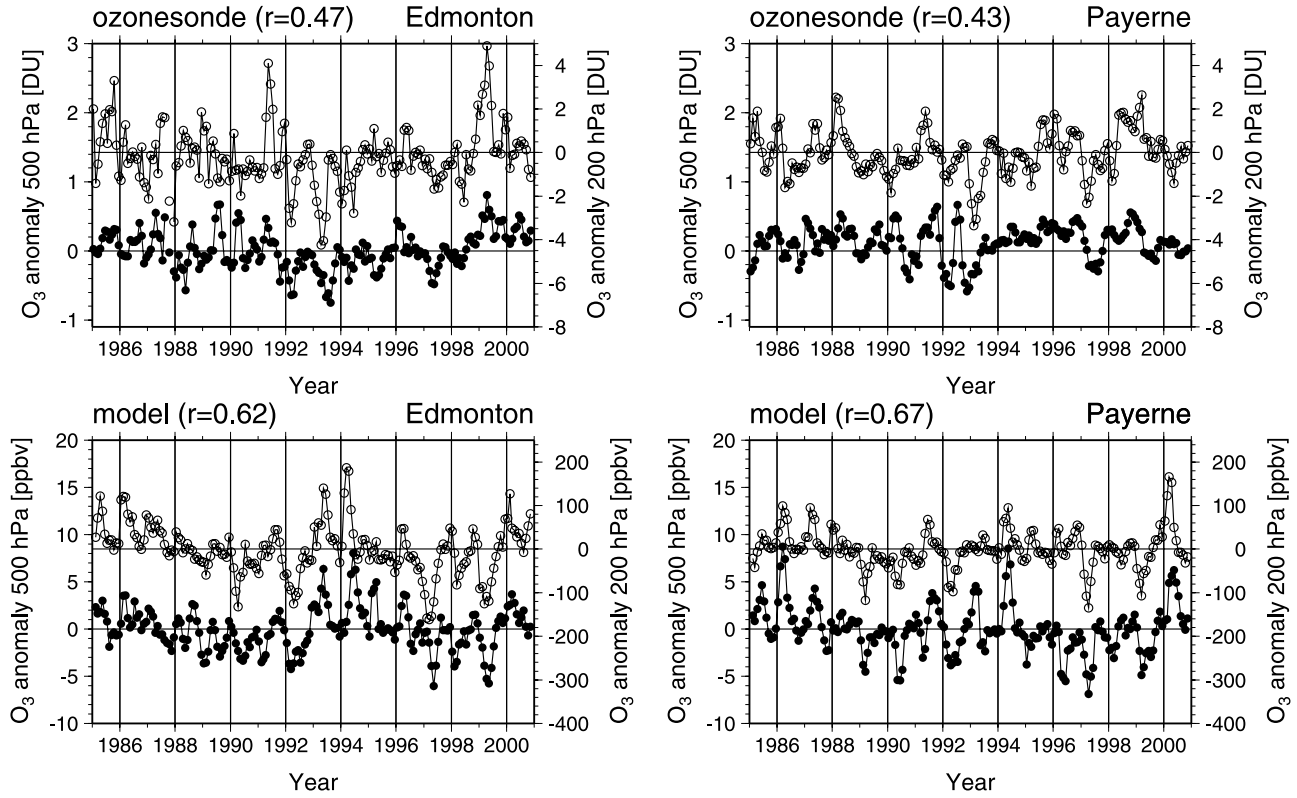

Figure 2. Monthly ozone anomalies observed by ozonesondes (in DU, top) and simulated by the model (in ppbv, bottom) at 500 hPa (black circles, scale on left) and 200 hPa (open circles, scale on right) for Edmonton and Payerne. The number (r) shows the correlation coefficient for two time series. A three month running mean was applied to the data.

from 1985 to 2000. A three month running mean was applied to the monthly anomalies of both the ozonesonde data and the model output.

3. Results

3.1. Seasonal Cycle of Ozone

[14] We evaluated the seasonal cycle of ozone simulated by the GSFC CTM using ozonesonde data as shown in Figure 1. The ozonesonde data are climatological monthly means from 1985 to 2000 at 200 hPa, 500 hPa, and 800 hPa, updated from *Logan* [1999]. The model output is averaged for the same period then interpolated to the ozonesonde levels. The model simulates lower stratospheric ozone very well at Resolute (75°N) and Hohenpeissenberg (48°N) at 200 hPa. For Boulder (40°N) and Tateno (36°N) at 200 hPa, the simulation underestimates the spring maximum of observed ozone but agrees well within the standard deviation of the observations. Note that the 200 hPa height is sometimes below the tropopause at these stations, particularly in late summer and fall. At 500 hPa and 800 hPa, the simulation overestimates observed ozone, with the largest discrepancies in winter and spring. The ozone maximum occurs a month earlier in the simulation than in the observations, except at high latitudes.

[15] Figure 1 also shows the separate contributions of O_3-trop and O_3-strat. At 200 hPa, O_3-strat dominates the ozone seasonality and O_3-trop levels are almost constant throughout the year. The O_3-trop contribution is most important in fall in midlatitudes: 43% at Hohenpeissenberg and ~90% at Boulder and Tateno in September. At 500 hPa, O_3-trop tends to peak later, and has a smaller amplitude, than observed ozone. At 800 hPa the seasonality of O_3-trop is similar to that of the observations, except for Tateno. The Japanese site is influenced by local pollution in the boundary layer, and also by the influx of low ozone from the tropics during the summer monsoon season.

[16] The results in Figure 1 imply that O_3-strat makes a significant contribution to the amount and seasonality of tropospheric ozone, with the largest influence in spring. The simulated contributions are: 37 ppbv (42% of ozone) at Resolute in May, 30 ppbv (39%) at Hohenpeissenberg in April, 27 ppbv (34%) at Boulder in April, and 20 ppbv (29%) at Tateno in March. The O_3-strat contribution in summer and fall is 10–20% at 500 hPa. O_3-strat contributes 18–20 ppbv at the 800 hPa level in winter. The simulation overestimates tropospheric ozone at 500 hPa by ~26% at Resolute and by ~16% at Hohenpeissenberg, Boulder and Tateno; the overestimate is somewhat larger at 800 hPa for Hohenpeissenberg and Boulder, ~25%. The model gives the correct amplitude and phase of the seasonal cycle, lending some confidence to the relative contributions of O_3-trop and O_3-strat. The CTM agrees better with observations at 800 hPa (but not at 500 hPa) with only O_3-trop, without any contribution from O_3-strat. It is likely that both the simulated O_3-trop and O_3-strat are biased high. Tropospheric ozone is higher than the ozonesonde data in the northern extratropics especially in winter-spring, in the

Table 1. Time Lagged Correlation Between Ozone Anomalies at 200 hPa and 500 hPa From Ozonesondes and Simulations at Edmonton and Payerne

	Edmonton		Payerne	
Lag (month)	Sonde	Model	Sonde	Model
0	0.47	0.62	0.43	0.67
1	0.46	0.66	0.37	0.68
2	0.44	0.62	0.31	0.57
3	0.33	0.50	0.23	0.38

GEOS-Chem model [e.g., *Fusco and Logan*, 2003] and in most other tropospheric models [*Stevenson et al.*, 2006].

[17] The mixing ratio of the O_3-strat tracers transported to the troposphere in this study is smaller than that estimated by *von Kuhlmann et al.* [2003] using a tropospheric CTM, but is larger than that in other tropospheric models [e.g., *Roelofs and Lelieveld*, 1997; *Fusco and Logan*, 2003; *Sudo and Akimoto*, 2007]. However, none of these models included a simulation of stratospheric ozone.

3.2. Correlation Between Lower Stratospheric Ozone and Tropospheric Ozone

[18] We show in Figure 2 the time series of monthly ozone anomalies for ozonesonde data and for the GSFC CTM, for the lower stratosphere (200 hPa) and midtroposphere (500 hPa) at Edmonton and Payerne. The ozonesonde time series at Edmonton shows anomalously low ozone in 1992 and 1993 and anomalously high ozone in 1991 and 1999 both for the lower stratosphere and midtroposphere. The behavior of ozone in the midtroposphere shows a resemblance to that in the lower stratosphere. We calculated the correlation coefficient (r) between the ozone time series in the lower stratosphere and in the midtroposphere for monthly anomaly data (referred as r(200, 500)), and found a significant correlation with r = 0.47 for Edmonton. For ozonesonde measurements at Payerne, the r(200, 500) is weaker than that for Edmonton. We also found a significant r(200, 500) in the simulated ozone time series both for Edmonton and Payerne. The simulation cannot represent the observed interannual variability of ozone, as it is driven by GCM meteorological data. However, the model provides typical interannual variability and evolving ozone depletion from 1980's to the early 1990's [*Stolarski et al.*, 2006].

[19] Figure 2 suggests that the variations in tropospheric ozone follow those in lower stratospheric ozone. Time lagged correlation analysis (Table 1) shows that, at Edmonton, r(200, 500) remains high even with a 2 month lag, while for Payerne it decreases with a lag of even 1 month. The model output also shows the correlations remaining high for 1–2 month lags at Edmonton, and while for Payerne the correlation remains high with a one month lag. Lagged correlations are discussed further below.

[20] We compare r(200, 500) as seen by ozonesondes and by the model for the 12 sonde locations in Figure 3. The modeled r(200, 500) vary with location in a similar manner to the observed r(200, 500), but with a high bias of 0.25–0.4 on average. One reason for the high bias of modeled r(200, 500) is that the simulated time series uses the same tropospheric production and loss rates and the same convective mass fluxes each year, so that these factors cannot introduce interannual variability. Also, the model includes no random errors, whereas there are both measurement errors and sampling issues in the observed time series. The measurements are based primarily on weekly measurements, except for the European stations [*Terao and Logan*, 2007].

[21] We found similar regional differences in r(200, 500) for the ozonesonde measurements and the simulations: high correlations over western North America (station code: 021, 024, and 067) and Europe (099 and 156), lower correlations over eastern North America (077 and 107), and no significant correlations over Japan (007, 012, and 014). Note that r values below ~0.2 are not statistically significant, for our sample size: n = 192 (12 months, 16 years) for the simulated time series for each grid and n = 155–191 for the sonde data (there are data gaps at some locations).

[22] Figure 4a shows the distribution of the simulated r(200, 500) in the northern extratropics (30°N–90°N), as well as observed r(200, 500). We found regional differences in r(200, 500) for the midlatitudes, with maximum values of >0.8 in the North Atlantic around 40°–50°N. The r(200, 500) values are relatively high over Europe. Other regions of high r(200, 500) are the eastern North Pacific and western North America. Conversely, r(200, 500) is low (<0.4) for south-east Asia, Japan, and the western Pacific. However, the 200 hPa layer is not in the lowermost stratosphere at the lower latitudes, near 30°–35°N, as shown by the seasonal cycle at Tateno (Figure 1). At high latitudes (>60°N), r(200, 500) increases with latitude. There are some low r(200, 500) spots (<0.4) along 60°N.

[23] We also show the results for the correlation between 500 hPa and 800 hPa, r(500, 800), and between 200 hPa and 800 hPa, r(200, 800) in Figures 4b and 4c. The r(500, 800) values are higher than r(200, 500) because air masses

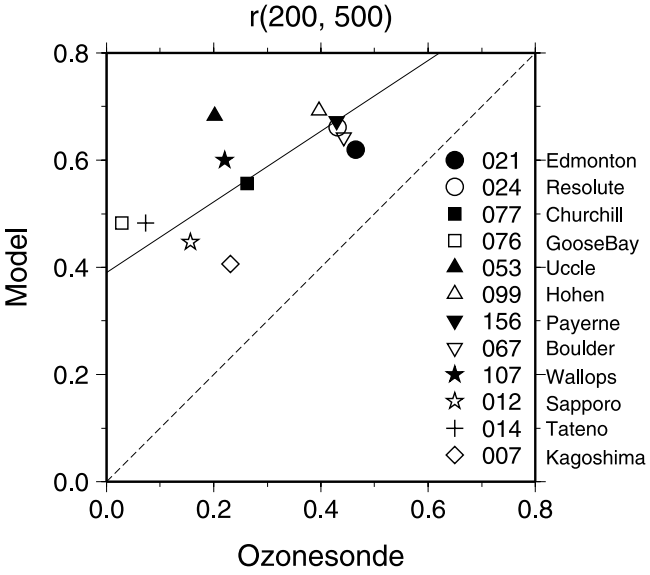

Figure 3. Comparison of the correlation coefficient between ozone anomalies at 200 hPa and at 500 hPa as seen by ozonesondes and model output. The figure shows the station code of each ozonesonde location (see text). The solid line shows a reduced major axis (RMA) regression fit (y = 0.66x + 0.39, r = 0.70), and the dashed line shows a nominal 1:1 relationship.

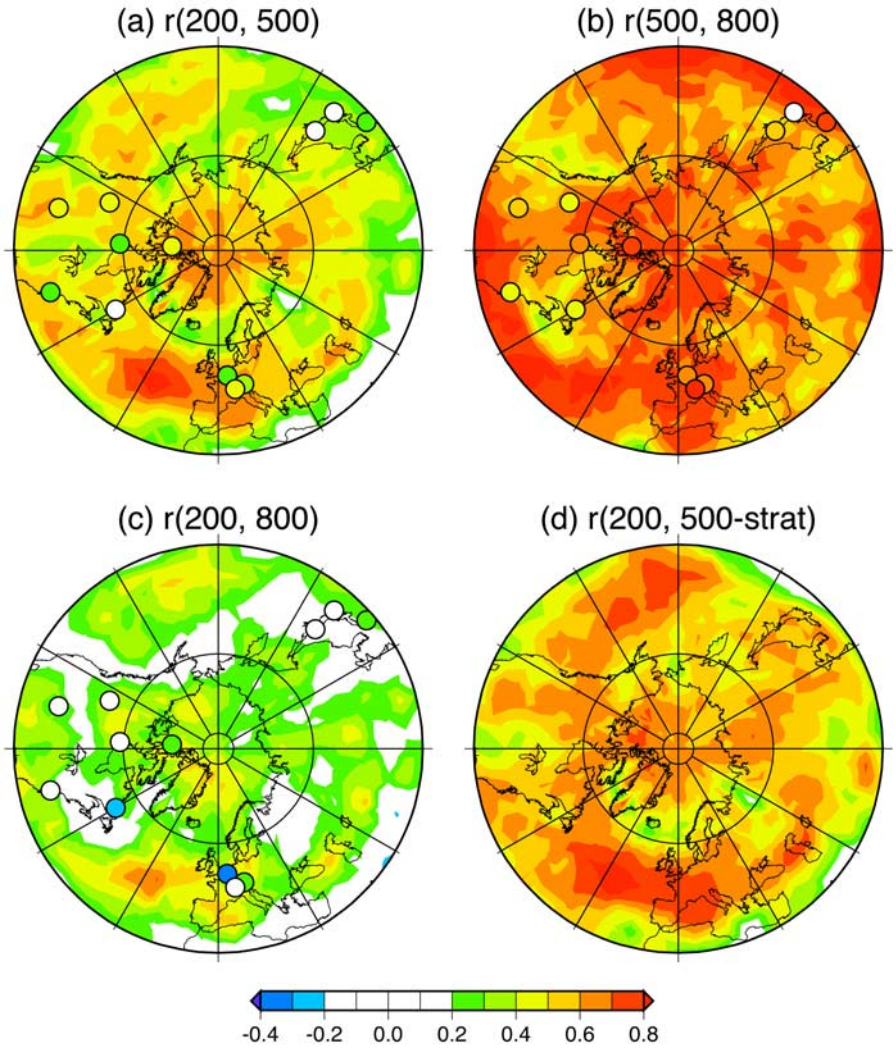

Figure 4. Correlation coefficient (r) between (a) ozone anomalies at 200 hPa and 500 hPa, (b) ozone anomalies at 500 hPa and 800 hPa, (c) ozone anomalies at 200 hPa and 800 hPa, and (d) ozone anomalies at 200 hPa and O_3-strat anomalies at 500 hPa. Results from ozonesondes are shown by circles with colors (Figures 4a–4c) and from the simulation by contours and colors (Figures 4a–4d). The contour interval is 0.1. The white area ($|r| < 0.2$) indicates the region with statistical significance less than 99%.

in the troposphere are generally well mixed. The r(200, 800) values are smaller than r(200, 500) likely because the influence of stratospheric ozone is smaller in the lower troposphere (Figure 1), but there is a similar spatial pattern. This indicates that the zonal structure in the midlatitudes is forced between the lower stratosphere and the troposphere, implying that this pattern is related to cross-tropopause input.

[24] To illustrate the effect of stratospheric input more directly, we show the correlation coefficient between ozone at 200 hPa and O_3-strat at 500 hPa (referred as r(200, 500-strat)) in Figure 4d. The spatial pattern of r(200, 500-strat) is almost the same as of r(200, 500) with higher r values. This confirms that the stratospheric input is responsible for the spatial pattern of r(200, 500). In the Pacific, the correlation is highest around 35°–45°N, 180°W and is of similar magnitude to the Atlantic maximum (Figure 4d), unlike the pattern for r(200, 500) where the maximum correlation in the Pacific is much smaller than that in the Atlantic. We found no significant positive correlation between ozone at 200 hPa and O_3-trop at 500 hPa (not shown).

[25] Figure 5 shows the seasonal dependence of r(200, 500). We selected the data from January to May for winter-spring and from July to November for summer-fall, then calculated r using 80 samples (5 months for 16 years) for the simulated time series for each season (less for the observations). The r values below ~0.3 are not statistically significant. The observed r(200, 500) values are higher for winter-spring than for summer-fall in all stations except for relatively low latitude stations, Kagoshima and Wallops. The simulated r(200, 500) values are higher for winter-spring than for year round data by 0.07 on average, and are lower for summer-fall by 0.22, and often insignificant. The spatial pattern of the year round r(200, 500) is clearly driven by that in winter-spring season.

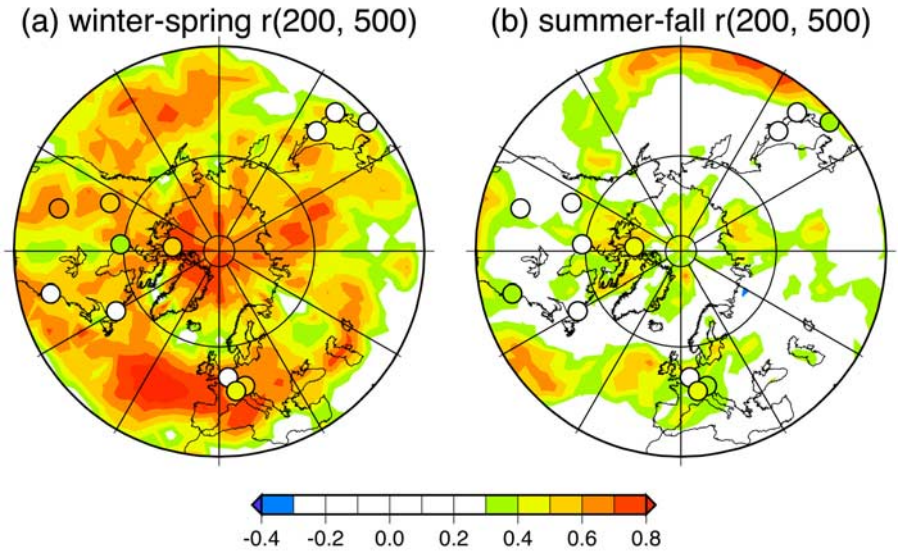

Figure 5. Same as Figure 4a but for (a) winter-spring (from January to May) and for (b) summer-fall (from July to November). The white area ($|r| < 0.3$) indicates the region with statistical significance less than 99%.

[26] We examined time lagged correlations for r(200, 500) in Figure 6. The figure shows differences between the correlation with zero lag and that with a 1 or 2 month lag. Positive (negative) values indicate that the correlation is higher (lower) with a time lag, and white shows regions with small changes (within ±0.05). At midlatitudes the best correlation is with zero lag. However for higher latitudes (>50°N over North America, >60°N over Europe, and >40°N over the Eastern Hemisphere), values of r(200, 500) are larger when ozone at 500 hPa lags that at 200 hPa by 1 or 2 months. The simulated spatial distribution of lagged correlations is supported by the results using ozonesonde data (also see Table 1). At Canadian stations the lagged correlation remains high for 1 or 2 months although it does not increase (unlike the simulation), while for Europe it drops with a lag.

4. Discussion and Conclusions

[27] We presented correlations of ozone time series between the lower stratosphere and the troposphere in the northern extratropics, using ozonesonde data and model output from the GSFC CTM driven by FVGCM products. Regions with the highest correlation are from the eastern

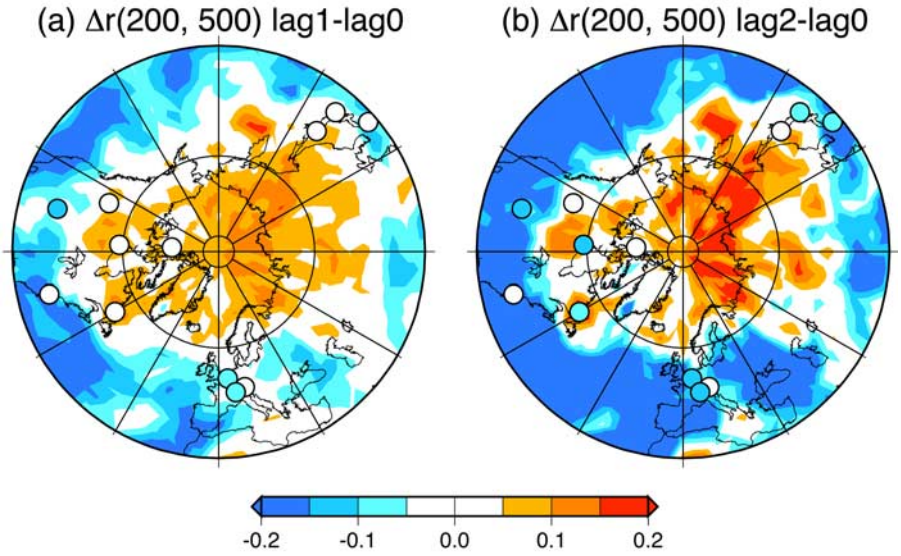

Figure 6. Time lagged correlations of r(200, 500) with (a) a 1 month lag and (b) a 2 month lag, plotted as differences from those with no time lag (Figure 4a). Results from ozonesondes are shown by circles with colors and from the simulation by contours and colors. The contour interval is 0.05.

Atlantic to Europe, from the eastern Pacific to the western United States, and in central Russia in winter-spring. This spatial pattern is due to stratospheric input into the troposphere. The model clearly supports the idea that interannual variability in tropospheric ozone can be driven by changes in input from the stratosphere, as found for Canada [*Tarasick et al.*, 2005] and central Europe [*Ordóñez et al.*, 2007], but our key finding is that the influence varies regionally. Canada and Europe are among the most highly correlated regions in the northern extratropics, and in such regions interannual variability and trends in tropospheric ozone may be influenced by any changes in lower stratospheric ozone. However, in the other regions, the stratospheric influence can be much smaller, and local sources and/or variability in transport from other source regions may play a dominant role in the variability of tropospheric ozone.

[28] Exchange between the lowermost stratosphere and the troposphere in the midlatitudes is driven by synoptic-scale processes, i.e., blocking, cutoff cyclones, and tropopause fold events (deep stratospheric intrusion), while in the high latitudes vertical transport by large-scale subsidence is the dominant mode, with a contribution also from horizontal poleward transport [*Holton et al.*, 1995; *Stohl et al.*, 2003]. The concentrated regions of synoptic eddy activity (i.e., storm tracks) are found in the Atlantic and in the Pacific in Northern Hemisphere winter [e.g., *Hoskins and Valdes*, 1990]. The Atlantic storm track is centered around 40°–50°N, 60°W, and the Pacific storm track is 40°–50°N, 180°E [*Nakamura*, 1992].

[29] The distribution of high r(200, 500) from the eastern Atlantic to Europe, with the clear maximum around 40°–50°N, 30°W, agrees well with the Atlantic storm track region. From the Pacific to western North America, we found high correlations associated with storm tracks only for r(200, 500-strat) in the central Pacific (35°–45°N, 180°W). This maximum is much smaller in the r(200, 500) field. One reason for the diminished correlation in the Pacific is that ozone of tropospheric origin in this region is more variable than in the Atlantic. The anomalies of O_3-trop at 500 hPa varies within ±5% in the central Atlantic but ±10% in the western Pacific. Export of ozone formed in East Asia to the Pacific is largest in winter and spring [*Liu et al.*, 2002], and there is considerable interannual variability in trans-Pacific transport of pollution from Asia [*Liu et al.*, 2003; *Liu et al.*, 2005].

[30] For midlatitudes, we showed that the r(200, 500) is highest with no time lag and that the r(200, 500) pattern appears only in winter-spring. The results support the idea that the zonal structure of r(200, 500) in midlatitudes is strongly linked to synoptic-scale storm tracks with transport on time scales less than a month. For higher latitudes, both the seasonality of r(200, 500) (higher in winter-spring) and the 1–2 month time-lag for the highest correlation are consistent with the characteristics of large-scale subsidence over the winter polar regions.

[31] Previous studies have estimated the cross-tropopause mass or ozone flux with a variety of approaches. *Olsen et al.* [2004] evaluated the mass and ozone flux across the tropopause using the GSFC CTM with a hemispheric mass balance method, and found that the largest diabatic flux of ozone from the stratosphere to the troposphere is in the Pacific and the Atlantic at 40°–60°N. *Hsu et al.* [2005] proposed another mass balance approach including a term for the horizontal gradient of tropospheric ozone and showed, from a CTM analysis, that the highest stratosphere-to-troposphere flux of ozone appears along the jet streams over the oceans in winter. *Sprenger and Wernli* [2003] calculated the cross-tropopause mass flux using ECMWF meteorological data for 1979–1993 with a Lagrangian approach. They showed zonal structure in the stratosphere-to-troposphere mass flux with maxima in the Atlantic and the Pacific in winter.

[32] The statistical method use here, examining correlations between ozone in the lower stratosphere and midtroposphere, is very simple compared with previous studies based upon physical processes [e.g., *Sprenger and Wernli*, 2003; *Olsen et al.*, 2004; *Hsu et al.*, 2005]. However, we have succeeded in diagnosing regions of STE of ozone using correlations from model output evaluated with observations. Our approach can be easily applied to other observations and to output from more sophisticated models that include time dependent emissions of ozone precursors and their chemistry as well as the evolution of stratospheric ozone.

[33] **Acknowledgments.** The ozonesonde data were provided by WOUDC, Samuel Oltmans, and Francis Schmidlin. We would like to thank Inna A. Megretskaia for her assistance with the ozonesonde data. This work was supported by the NASA/ACMAP program.

References

Douglass, A. R., M. R. Schoeberl, R. B. Rood, and S. Pawson (2003), Evaluation of transport in the lower tropical stratosphere in a global chemistry and transport model, *J. Geophys. Res.*, *108*(D9), 4259, doi:10.1029/2002JD002696.

Fiore, A., D. J. Jacob, H. Liu, R. M. Yantosca, T. D. Fairlie, and Q. Li (2003), Variability in surface ozone background over the United States: Implications for air quality policy, *J. Geophys. Res.*, *108*(D24), 4787, doi:10.1029/2003JD003855.

Fusco, A. C., and J. A. Logan (2003), Analysis of 1970–1995 trends in tropospheric ozone at Northern Hemisphere midlatitudes with the GEOS-CHEM model, *J. Geophys. Res.*, *108*(D15), 4449, doi:10.1029/2002JD002742.

Holton, J. R., P. H. Haynes, M. E. McIntyre, A. R. Douglass, R. B. Rood, and L. Pfister (1995), Stratosphere-troposphere exchange, *Rev. Geophys.*, *33*(4), 403–440.

Hoskins, B. J., and P. J. Valdes (1990), On the existence of storm-tracks, *J. Atmos. Sci.*, *47*(15), 1854–1864.

Hsu, J., M. J. Prather, and O. Wild (2005), Diagnosing the stratosphere-to-troposphere flux of ozone in a chemistry transport model, *J. Geophys. Res.*, *110*, D19305, doi:10.1029/2005JD006045.

Kiehl, J. T., J. J. Hack, G. B. Bonan, B. A. Boville, D. L. Williamson, and P. J. Rasch (1998), The National Center for Atmospheric Research Community Climate Model: CCM3, *J. Clim.*, *11*, 1131–1149.

Lelieveld, J., and F. J. Dentener (2000), What controls tropospheric ozone?, *J. Geophys. Res.*, *105*, 3531–3551.

Lin, S.-J. (2004), A vertically Lagrangian finite-volume dynamical core for global models, *Mon. Weather Rev.*, *132*, 2293–2307.

Lin, S.-J., and R. B. Rood (1996), Multidimensional flux form semi-Lagrangian transport schemes, *Mon. Weather Rev.*, *124*, 2046–2070.

Lin, S.-J., and R. B. Rood (1997), An explicit flux-form semi-Lagrangian shallow water model on the sphere, *Q. J. R. Meteorol. Soc.*, *123*, 2477–2498.

Liu, H., D. J. Jacob, L. Y. Chan, S. J. Oltmans, I. Bey, R. M. Yantosca, J. M. Harris, B. N. Duncan, and R. V. Martin (2002), Sources of tropospheric ozone along the Asian Pacific Rim: An analysis of ozonesonde observations, *J. Geophys. Res.*, *107*(D21), 4573, doi:10.1029/2001JD002005.

Liu, H., D. J. Jacob, I. Bey, R. M. Yantosca, B. N. Duncan, and G. W. Sachse (2003), Transport pathways for Asian pollution outflow over the Pacific: Interannual and seasonal variations, *J. Geophys. Res.*, *108*(D20), 8786, doi:10.1029/2002JD003102.

Liu, J., D. L. Mauzerall, and L. W. Horowitz (2005), Analysis of seasonal and interannual variability in transpacific transport, *J. Geophys. Res.*, *110*, D04302, doi:10.1029/2004JD005207.

Logan, J. A. (1994), Trends in the vertical distribution of ozone: An analysis of ozonesonde data, *J. Geophys. Res.*, *99*, 25,553–25,585.

Logan, J. A. (1999), An analysis of ozonesonde data for the lower stratosphere: Recommendations for testing models, *J. Geophys. Res.*, *104*, 16,151–16,170.

Logan, J. A., et al. (1999), Trends in the vertical distribution of ozone: A comparison of two analyses of ozonesonde data, *J. Geophys. Res.*, *104*, 26,373–26,399.

Nakamura, H. (1992), Midwinter suppression of baroclinic wave activity in the Pacific, *J. Atmos. Sci.*, *49*, 1629–1642.

Olsen, M. A., M. R. Schoeberl, and A. R. Douglass (2004), Stratosphere-troposphere exchange of mass and ozone, *J. Geophys. Res.*, *109*, D24114, doi:10.1029/2004JD005186.

Oltmans, S. J., et al. (2006), Long-term changes in tropospheric ozone, *Atmos. Environ.*, *40*, 3156–3173.

Ordóñez, C., D. Brunner, J. Staehelin, P. Hadjinicolaou, J. A. Pyle, M. Jonas, H. Wernli, and A. S. H. Prévôt (2007), Strong influence of lowermost stratospheric ozone on lower tropospheric background ozone changes over Europe, *Geophys. Res. Lett.*, *34*, L07805, doi:10.1029/2006GL029113.

Rayner, N. A., D. E. Parker, E. B. Horton, C. K. Folland, L. V. Alexander, D. P. Rowell, E. Kent, and A. Kaplan (2003), Global analyses of sea surface temperature, sea ice, and night marine air temperature since the late nineteenth century, *J. Geophys. Res.*, *108*(D14), 4407, doi:10.1029/2002JD002670.

Roelofs, G.-J., and J. Lelieveld (1997), Model study of the influence of cross-tropopause O_3 transports on tropospheric O_3 levels, *Tellus, Ser. B*, *49*, 38–55.

Sprenger, M., and H. Wernli (2003), A northern hemispheric climatology of cross-tropopause exchange for the ERA15 time period (1979–1993), *J. Geophys. Res.*, *108*(D12), 8521, doi:10.1029/2002JD002636.

Stevenson, D. S., et al. (2006), Multimodel ensemble simulations of present-day and near-future tropospheric ozone, *J. Geophys. Res.*, *111*, D08301, doi:10.1029/2005JD006338.

Stohl, A., H. Wernli, P. James, M. Bourqui, C. Forster, M. A. Liniger, P. Seibert, and M. Sprenger (2003), A new perspective of stratosphere-troposphere exchange, *Bull. Am. Meteorol. Soc.*, *84*, 1565–1573.

Stolarski, R. S., A. R. Douglass, S. Steenrod, and S. Pawson (2006), Trends in stratospheric ozone: Lessons learned from a 3D chemical transport model, *J. Atmos. Sci.*, *63*(3), 1028–1041.

Strahan, S. E., and A. R. Douglass (2004), Evaluating the credibility of transport processes in simulations of ozone recovery using the Global Modeling Initiative three-dimensional model, *J. Geophys. Res.*, *109*, D05110, doi:10.1029/2003JD004238.

Sudo, K., and H. Akimoto (2007), Global source attribution of tropospheric ozone: Long-range transport from various source regions, *J. Geophys. Res.*, *112*, D12302, doi:10.1029/2006JD007992.

Tarasick, D. W., V. E. Fioletov, D. I. Wardle, J. B. Kerr, and J. Davies (2005), Changes in the vertical distribution of ozone over Canada from ozonesondes: 1980–2001, *J. Geophys. Res.*, *110*, D02304, doi:10.1029/2004JD004643.

Terao, Y., and J. A. Logan (2007), Consistency of time series and trends of stratospheric ozone as seen by ozonesonde, SAGE II, HALOE, and SBUV (/2), *J. Geophys. Res.*, *112*, D06310, doi:10.1029/2006JD007667.

von Kuhlmann, R., M. G. Lawrence, P. J. Crutzen, and P. J. Rasch (2003), A model for studies of tropospheric ozone and nonmethane hydrocarbons: Model description and ozone results, *J. Geophys. Res.*, *108*(D9), 4294, doi:10.1029/2002JD002893.

World Meteorological Organization (WMO) (2003), Scientific assessment of ozone depletion: 2002, *Global Ozone Res. and Monit. Proj. Rep. 47*, Geneva.

World Meteorological Organization (WMO) (2007), Scientific assessment of ozone depletion: 2006, *Global Ozone Res. and Monit. Proj. Rep. 50*, Geneva.

Zbinden, R. M., J.-P. Cammas, V. Thouret, P. Nédélec, F. Karcher, and P. Simon (2006), Mid-latitude tropospheric ozone columns from the MOZAIC program: climatology and interannual variability, *Atmos. Chem. Phys.*, *6*, 1053–1073.

A. R. Douglass and R. S. Stolarski, Atmospheric Chemistry and Dynamics Branch, NASA Goddard Space Flight Center, Greenbelt, MD 20771, USA.

J. A. Logan, School of Engineering and Applied Sciences, Harvard University, 29 Oxford Street, Cambridge, MA 02138, USA. (jlogan@seas.harvard.edu)

Y. Terao, Center for Global Environmental Research, National Institute for Environmental Studies, 16-2 Onogawa, Tsukuba, Ibaraki 305-8506, Japan. (yterao@nies.go.jp)